AD

TECHNICAL REPORT ARCCB-TR-03008

EROSION MODELING OF THE HIGH CONTRACTION CHROMIUM PLATED CRUSADER GUN SYSTEM

S. SOPOK
C. RICKARD
G. PFLEGL
P. O'HARA
S. DUNN
D. COATS

JUNE 2003

US ARMY ARMAMENT RESEARCH,
DEVELOPMENT AND ENGINEERING CENTER
Close Combat Armaments Center
Benét Laboratories
Watervliet, NY 12189-4000

DISCLAIMER

The findings in this report are not to be construed as an official Department of the Army position unless so designated by other authorized documents.

The use of trade name(s) and/or manufacturer(s) does not constitute an official endorsement or approval.

DESTRUCTION NOTICE

For classified documents, follow the procedures in DoD 5200.22-M, Industrial Security Manual, Section II-19, or DoD 5200.1-R, Information Security Program Regulation, Chapter IX.

For unclassified, limited documents, destroy by any method that will prevent disclosure of contents or reconstruction of the document.

For unclassified, unlimited documents, destroy when the report is no longer needed. Do not return it to the originator.

REPORT DOCUMENTATION PAGE

Form Approved
OMB No. 0704-0188

1. AGENCY USE ONLY (*Leave Blank*)	2. REPORT DATE	3. REPORT TYPE AND DATES COVERED
	June 2003	Final

4. TITLE AND SUBTITLE
EROSION MODELING OF THE HIGH CONTRACTION CHROMIUM PLATED CRUSADER GUN SYSTEM

5. FUNDING NUMBERS
PRON No. TU1D1F261ABJ

6. AUTHORS
S. Sopok, C. Rickard, G. Pflegl (Battelle Laboratories, Watervliet, NY), P. O'Hara (Elmhurst Research, Albany, NY), S. Dunn (Software and Engineering Associates, Inc., Carson City, NV), and D. Coats (Software and Engineering Associates, Inc., Carson City, NV)

7. PERFORMING ORGANIZATION NAME(S) AND ADDRESS(ES)
U.S. Army ARDEC
Benet Laboratories. AMSTA-AR-CCB-O
Watervliet, NY 12189-4050

8. PERFORMING ORGANIZATION REPORT NUMBER
ARCCB-TR-03008

9. SPONSORING / MONITORING AGENCY NAME(S) AND ADDRESS(ES)
U.S. Army ARDEC
Close Combat Armaments Center
Picatinny Arsenal, NJ 07806-5000

10. SPONSORING / MONITORING AGENCY REPORT NUMBER

11. SUPPLEMENTARY NOTES
Presented at the 38th AIAA Joint Propulsion Conference, Indianapolis, IN, 7-10 July 2002.
Published in proceedings of the conference.

12a. DISTRIBUTION / AVAILABILITY STATEMENT
Approved for public release; distribution unlimited.

12b. DISTRIBUTION CODE

13. ABSTRACT (*Maximum 200 words*)

Thermal-chemical-mechanical erosion modeling predictions are given for the high contraction chromium plated Crusader gun system based on extensive cannon firing, inspection, characterization, and experimental data. This effort was conducted for the Army's Crusader Program Manager Office and managed by Applied Ordnance Technology. The authors carefully protect proprietary technical data that was provided by various government and nongovernment partners involved in this effort. Key gun system details include the 155-mm 56 caliber rifled XM297 cannon with a 1400 in^3 chamber, zone six combustible case-type modular artillery charge, triple-base propellant, an approximately 100-pound M549-like projectile, its nominal obturator, maximum chamber pressure of approximately 55 kpsi, 0.005-inch thick high contraction chromium plate on both the lands and grooves of the steel, ambient temperature conditioning, no in-wall barrel cooling, decoppering and flash additives, and no wear additives. This XM297 gun system can be condemned on erosion due to loss of velocity, fuse malfunction, rotating band wear, excessive body engraving, and loss of accuracy. A provisional 0.105-inch diametric origin erosion limit (usually at 12:00 to 6:00 peak) applies in the absence of these condemning effects as measured by pullover or star gages. Most key cannons were near this provisional diametric erosion limit and were destructively characterized resulting in moderately high confidence erosion predictions. Thermal and erosion predictions are made for five different firing rate scenarios from 1 round per hour to 8 rounds per minute. For the 1 round per hour firing rate scenario, we predict that it requires approximately 1520 EFCs to achieve arbitrary 0.100-inch wall erosion at the 12:00 o'clock peak eroded origin position and 1005 EFCs to achieve arbitrary 0.100-inch diametric erosion at the 12:00 to 6:00 o'clock peak eroded origin position. For the 8-round per minute (recurring15-round groups) firing rate scenario, we predict that it requires approximately 450 EFCs to achieve arbitrary 0.100-inch wall erosion at the 12:00 o'clock peak eroded origin position and 400 EFCs to achieve arbitrary 0.100-inch diametric erosion at the 12:00 to 6:00 o'clock peak eroded origin position. The reduced erosion life of the higher rate of fire scenarios is due to obturator blowby that causes accelerated groove erosion during the first six inches of travel.

14. SUBJECT TERMS
Advanced Artillery Systems, Cannon Bore Erosion, Thermal-Chemical-Mechanical Erosion, Erosion Mechanisms, Erosion Modeling, Coating-Substrate Erosion Modeling, Erosion Predictions

15. NUMBER OF PAGES
31

16. PRICE CODE

17. SECURITY CLASSIFICATION OF REPORT	18. SECURITY CLASSIFICATION OF THIS PAGE	19. SECURITY CLASSIFICATION OF ABSTRACT	20. LIMITATION OF ABSTRACT
UNCLASSIFIED	UNCLASSIFIED	UNCLASSIFIED	UL

TABLE OF CONTENTS

LIST OF ILLUSTRATIONS

ACKNOWLEGEMENTS

The authors are pleased to acknowledge the help of numerous colleagues for their technical guidance in many phases of this work including: E. Hyland, S. VanDyke-Resitifo, A. Wakulenko, and J. Underwood of Benet Labs; S. Coladonato of Applied Ordnance Technology (Waldorf, MD); B. Anderson of United Defense L.P. (Minneapolis, Minnesota); J. Rutkowski and T. Grieg of the PM-Crusader Office; and T. Sterlacci of the FCS-NLOS Office. The authors are also pleased to acknowledge the preliminary modeling efforts of M. Witherell, D. Bleau, and M. Leach of Benet Labs, as well as the nondestructive testing efforts of D. Le of the Army Test Center (Yuma Proving Ground, AZ).

INTRODUCTION

There are a number of typical reasons why erosion modeling is used to predict the erosion life of advanced prototype gun systems based on limited erosion data including:

- Only a small number of cannons have been fired.
- These cannons are less than half way through their erosion life.
- There is a mix of charges and zones fired.
- Firing was conducted with a mix of round conditioning temperatures.
- Firing was conducted with a mix of projectiles.
- Firing was conducted with a mix of firing rate scenarios.

Our erosion modeling provides a comprehensive framework for making the best possible erosion predictions by incorporating all of the data from a given advanced prototype gun system's firings, inspections, characterizations, and experiments.

This work was prompted by the origin erosion condemnation of a prototype high contraction (HC) chromium plated XM297 cannon with no in-wall cooling that fired about 200 rapid fire rounds at 8 rounds per minute in 15-round bursts equaling about 200 EFCs using a zone six prototype charge and projectile. This prototype charge consisted of an ambient temperature-conditioned combustible case-type modular artillery charge with triple-base propellant that produced a chamber pressure of approximately 55 kpsi and had decoppering and flash additives, but no wear additives. The prototype projectile was an M549-like projectile with its nominal obturator. This cannon had a total of about 370 EFCs since it previously fired about 170 EFCs at much lower firing rates resulting no erosion.

Never before seen rapid firing-induced groove erosion apparently caused this prototype XM297 cannon to erode to condemnation in less than a tenth of its expected life. A pullover gage is used in the field to measure origin erosion on this cannon. A pullover gage misses this erosion, since origin groove erosion occurred in the near absence of origin land erosion. In addition, never before seen deep origin groove pits caused serious fatigue concerns for the artillery community. We conducted erosion mechanism determinations, erosion modeling, and erosion predictions for the Army's Crusader Program Manager to address these concerns.

COMPUTATIONAL AND EXPERIMENTAL METHODS

Our cannon erosion model is used to predict wall temperatures and thermal-chemical-mechanical erosion profiles in cannons (ref 1). Statistical distributions exist around these various wall temperature and erosion predictions as a function of position, time, round type, and round history. This erosion model includes:

- CCET thermochemical cannon model (refs 1,2)
- XNOVAKTC interior ballistics cannon model (refs 1,3)
- MABL boundary layer cannon model (refs 1,4)
- MACE thermal and erosion cannon model (refs 1,5,6)

This thermal-chemical-mechanical erosion model has been comprehensively extended for refractory metal-coated cannon bores with steel substrates (ref 6). These erosion predictions are guided and calibrated by substantial gun system firing data and laboratory analyses of fired specimens. English units are used exclusively throughout this report as requested by the customer.

Pressure gage, radar, thermocouple, metallographic, and kinetic rate data are used to calibrate these models. Important model inputs include nondestructive and destructive laboratory microscopic materials and chemical analyses of fired cannon specimens. Substrate exposure, coating loss, cracks, pits, interfaces, voids, surfaces, crack/pit frequency, crack/pit width, coating platelet width, wall layers, residues, reactions, diffused species, and phase changes all as a function of position, time, and round history provide important model inputs.

RESULTS AND DISCUSSION

The first firing rate scenario is at 1 round per hour (rph) and includes the recurrence of a 70°F initial temperature by firing a single round and then cooling the gun bore back to ambient. The second through fifth firing rate scenarios are at x rounds per minute (rpm) with x = 2, 4, 6, and 8, and include the recurrence of a 70°F initial temperature by firing a 15-round group at x rpm and then cooling the gun bore back to ambient. Extensive nondestructive and destructive inspections and characterizations were conducted on gun tubes that have experienced these specific firing scenarios. Erosion mechanisms were determined for these specific firing rate scenarios.

The thermochemical cannon model requires initial chemical and materials inputs from the gun system to calculate gas and gas/wall thermochemical data for the interior ballistics, boundary layer, and thermal and erosion models. These measured thermochemical data are used to calibrate the calculation for gas products, gas/wall products, and gas/wall reaction rates.

Blake thermochemical names (ref 2) are used to define the standard triple-base propellant that approximately consists of NC1260 at 28%, NG at 22%, NQ at 47%, and other constituents at 3%. Measured thermochemical data are used to calibrate the calculation for gas/gas products.

For this gun system, our inspections of, characterizations of, and experiments on fired cannons have provided required composition and materials input data for the thermochemical model. These input data are for both cannons having fired only recurring single rounds and cannons having fired recurring rapid-fired rounds. These data include composition, material properties, subsurface exposure, degradation mechanisms, and gas/wall kinetic rate inputs. For this gun system case, similar thermochemical model data are provided for the approximately 100-pound M549-like projectile, its nominal obturator, and its nominal rotating band.

The interior ballistics cannon model uses thermochemistry model output and gun system defining inputs to calculate the time-dependent core flow data for the boundary layer model. Measured pressure gage and muzzle velocity data from this gun system are used to calibrate the time-dependent core flow calculation.

Figures 1 through 3 give XNOVAKTC interior ballistic model results for this gun system. These figures respectively give maximum values of gas pressure (P_g), gas temperature (T_g), and gas velocity (V_g) as a function of bore travel in about 50-inch axial position increments. Maximum values are shown instead of time-dependent data.

Figure 4 shows the MACE nonreacting thermal analysis predicted for this gun system. Input data are required for both cannons having fired only recurring single rounds and cannons having fired recurring rapid-fired rounds. This figure shows predicted maximum bore surface temperatures for the HC chromium bore surface as a function of selected axial positions at the first, eighth, and fifteenth rounds of an 8 rpm firing rate. Maximum values are shown instead of calculated time-dependent data to compare these three round numbers. By this purely thermal analysis, the origin position (full commencement of rifling 47.0 inches from the rear face of the tube [RFT] 294.7 inches from the front face of the muzzle) has the peak bore surface temperature for this gun system, which diminishes with increasing travel. The XM297 gun bore circumference has 48 one-eighth inch wide lands and 48 one-quarter inch wide grooves.

The MABL boundary layer cannon model uses thermochemistry and interior ballistics model outputs to calculate boundary layer characteristics for the thermal and erosion model. Figures 5 and 6 give the MABL boundary layer model results for this gun system. These figures respectively give time-dependent values of recovery enthalpy (H_r) and cold wall heat flux (Q_{cw}) as a function of time at the 47-inch from RFT peak bore surface axial position. Since ablative cooling was ignored, the boundary layer inclusion of the 2420°F combustible case gas cooling effects and its turbulent gas mixing and heating effects was not evaluated.

The CCET thermochemistry cannon model uses initial chemical and materials input to calculate gas/wall thermochemistry data for the thermal and erosion code. Measured thermochemical data are used to calibrate the calculation for gas/wall products and gas/wall reaction rates. Figure 7 gives the CCET thermochemical model results for this gun system. Simplified mean values are shown for the reacting gas/wall enthalpy (H_{gw}) as a function of wall temperatures (T_{wall}) for the HC chromium plate and steel substrate wall materials instead of the broad spectrum of calculated values. The H_{gw} of the steel substrate progressively diverges from its initial path due to the oxidation at the steel transformation and oxidation onset temperature ($T_{t\text{-}ox}$) of about 1340°F.

Using nondestructive and destructive laboratory microscopic materials/chemical analyses of fired cannon specimens, we measure the achievement of and level above these reaction thresholds as a function of position, time, and round history. This bore coating erosion model requires measurable gas/wall bore coating and steel substrate reactivity data as functions of pressure, temperature, and velocity. These data are from the literature and in-house measurements for each gun system material/configuration using specialized gas/wall kinetic rate testers.

The MACE thermal and erosion cannon model uses thermochemistry model output, boundary layer model output, material properties input, and firing history-scenario input. This model calculates wall temperature profiles and thermal-chemical-mechanical wall erosion

profiles. The predicted results are given as a function of axial position, time, round type, and firing history-scenario.

The following data types are used to calibrate the wall thermal and erosion calculation:

- Measured gas/wall kinetic rate function input data
- Measured thermocouple input data
- Measured destructive/nondestructive microscopic coating and steel loss input data (cracks, pits, interfaces, surfaces)
- Measured destructive reaction/diffusion/phase change degradation layer input data (cracks, pits, interfaces, surfaces)

Input data are required for both cannons having fired only recurring single rounds and cannons having fired recurring rapid-fired rounds.

Experimentally measured chemical gas/wall kinetic rate function data are used to calibrate the thermochemical calculation and transform this chemical equilibrium calculation into a partial chemical kinetic calculation. Various techniques are used to chemically characterize and further guide this gas/wall kinetics calibration including wall layers (crack, pit, interface, surface) for phase change degradation (carburized white layer and heat-affected zones), chemical reaction degradation (oxidation and sulfidation) of the gun steel substrate under the chromium plate, subsurface void residues, and surface residues. Thermocouple and metallographic data are used to calibrate the wall thermal profile calculation.

Based on the latest nondestructive and destructive cannon characterization data for this gun system, Figures 8 and 9 give typical gun steel substrate exposure for the XM297 cannon at the 47-, 50- and 53-inch from RFT positions. For this gun system, these data are from a small sampling of both low and high rate of fire HC chromium plated XM297 cannons that have typical cracking, pitting, chromium plate loss, and erosion. Nondestructive substrate exposure measurements were performed by a 70x magnifying borescope with a calibrated scale, a video borescope, and an erosion gage. Erosion depth was performed by a pullover and star gage. These nondestructive measurements are based on the verified assumption that substrate exposure is approximately equal at the surface and interface. For condemned cannons, erosion characterizations were destructively conducted on surfaces and cross-sections of sectioned cannons by a metallograph and scanning electron microscope (SEM). Peak erosion is at the origin and diminishes completely six inches down-bore of the origin. Bore position-dependent and equivalent erosion life-dependent substrate exposure measurements of specimens from fired cannons include axial and circumferential crack/pit frequency, axial and circumferential crack/pit width, and axial and circumferential platelet width.

Figure 8 shows percent groove substrate exposure versus the selected origin axial positions for this gun system at 8 rpm, and the 10:00 to 2:00 clock position. These were measured at 1% (nondestructively measured at post-proofing), 50% (exponentially estimated from nondestructive measurements), 80% (exponentially estimated from nondestructive measurements), and 100% (nondestructively measured and destructively measured near erosion condemnation) of this equivalent ambient-conditioned zone six charge erosion life. Groove

erosion dominated over land erosion for this gun system's 8 rpm firing rate, based on the rate of groove erosion in tubes 8, 9 and 12.

Similarly, Figure 9 shows percent land substrate exposure versus the selected origin axial positions for this gun system for 1 rph, and the 10:00 to 2:00 clock position. These were measured at 1% (nondestructively measured at post-proofing), 50% (exponentially estimated from nondestructive measurements), 80% (exponentially estimated from nondestructive measurements), and 100% (nondestructively measured and destructively measured near erosion condemnation) of this equivalent ambient-conditioned zone six charge erosion life. Land erosion dominated over groove erosion for this gun system's 1 rph firing rate, based on the rate of land erosion in tubes 2, 7, and a number of other tubes that experienced this low firing rate. Substrate exposure for lands would have much higher percentages if they were only for the driving edge and not averaged over the whole land.

This gun system's erosion mechanism onset and progression has many components. Crack-related firing damage leading to erosion includes major chromium plate heat checking cracks, smaller microcracks within chromium platelets, and major/minor steel substrate cracks. Thermal-related firing damage leading to erosion includes grain growth near chromium plate surface, 1920°F recrystallization deeper in chromium plate, and 1340°F substrate steel transformations and a heat-affected zone near the steel interface. Thermochemical-related firing damage leading to erosion includes corrosion and scale damage very near the steel interface in the form of an oxidation layer and white layer. We have detailed all of these erosion mechanisms and components in previous work we conducted on other rifled artillery, smoothbore tanks, and rifled medium caliber cannons (refs 1,6).

One erosion mechanism component is HC chromium radial cracking, heat checking, and formation of a semi-porous crack network within the platelets. Gun bore HC chromium plate has a network of electroplating and associated heat-treatment-induced radial microcracks that usually do not all extend into the steel substrate. With limited firing, some of these radial microcracks widen and extend to/beyond the steel interface forming well-defined platelets in the HC chromium coating known as heat-checking cracks. Most of these radial microcracks are within the platelets and they do not result in widening, but instead form a semi-porous microcrack network that extends to the steel interface. Continued firing produces HC chromium plate contraction or shrinkage that causes radial heat-checking cracks to permanently widen. Firing pressure dilation initially opens these major radial cracks wider, but about a millisecond later thermal expansion of the coating recloses these cracks. Radial heat-checking cracks and microcracks within platelets are less frequent in low contraction (LC) chromium plate that tends to extend erosion life.

Numerous reasons explain this permanent widening of HC chromium radial heat-checking cracks. High contraction chromium plate radial heat checking cracks widen due to thermally induced outgassing of nonmetallics out of the exposed coating surfaces and through the semi-porous microcrack network within platelets. Outgassing is controlled by time above various temperature thresholds. This outgassing is less prevalent in LC chromium plate due to a much-reduced microcrack network within its platelets. High contraction chromium plate radial heat-checking cracks also widen due to radial crack wall yielding due to thermally induced

expansion forces on the brittle yielding sidewalls of HC chromium platelets. This yielding is much less for its more ductile LC chromium plate counterpart. High contraction chromium plate radial heat-checking cracks also widen due to thermally induced platelet sidewall transition from a less efficiently packed nonequilibrium state to a more efficient packing equilibrium state (not a transformation volume change) controlled by time above various temperature thresholds.

Recent work by Underwood (ref 8) includes a much-needed quantitative thermal-mechanical erosion model where different width radial heat-checking cracks are on opposite sides of a fully adhered HC chromium platelet attached to the steel substrate. This model predicts the interfacial forces required to shear this platelet from the substrate based on the thermally induced expansion forces on the yielding sidewalls of HC chromium platelets that widen these radial heat-checking cracks. This shearing model predicts the extreme upper limit of forces (excellent adhesion) required to shear a chromium-plated platelet from its fully adhered metal-metal bonded steel substrate. The shearing model also predicts the extreme lower limit of forces (very poor adhesion) required to shear a chromium-plated platelet from its nonadhered physically attached steel substrate.

Our thermal-chemical-mechanical erosion model addresses the substantial reduction of required interfacial shearing forces due to interfacial degradation. We have previously detailed that degradation of the platelet-substrate interface plus mild shearing is what actually happens in gun systems (refs 1,6). Shearing alone is not enough to take chromium platelets off the steel substrate. Underwood's model sets much needed boundaries on these shearing forces enabling us to better compute reduced shearing forces due to interfacial degradation.

Another erosion mechanism component is the exposure of the interfacial steel substrate to thermochemical degrading combustion gases. With limited firing, HC chromium plate's radial heat-checking cracks quickly extend to the steel interface and widen, providing progressively increasing paths for these combustion gases to chemically degrade and form voids in the exposed steel interface at the base of these cracks filled with a semi-metallic to nonmetallic interfacial oxidization layer. Although there is little convective heating in these narrow cracks, the substrate steel at the base of these heat-checking cracks reacts with the high-pressure combustion gases for as long as the substrate steel temperature is above a given reaction threshold. These interfacial voids occur at the base of most heat-checking cracks and reduce platelet-substrate adhesion around the interfacial edges of the platelet-substrate interface. The oxidation layer-filled voids at the base of heat-checking cracks partially detach the chromium platelet edges from the steel substrate, and it does not matter whether the void thickness is a thousand, million, or billon atoms thick since the adhesion is still zero at any atomic thickness. Interfacial void link-up around the edges of the platelets accelerates the loss of platelet-substrate adhesion leading to platelet spalling. These combustion gas paths are confined to the limited cross-sectional area that includes the platelet edges. Each round fired provides a fresh volume of thermochemical degrading high-pressure combustion gases to fill each radial crack extending to the steel interface at the edges of platelets. The heat-checking cracks form interconnecting "canyons" and each round fired provides a high-velocity flow of the turbulent degrading combustion gases (gas wash flow) across the substrate steel at the base of these canyons that continuously refreshes the exposed interfacial surface. Polished bore cross-sections of heat-checking cracks and

thermochemically damaged steel substrate voids at the base of these cracks typically require 100x magnification.

Also with limited firing, HC chromium plate's semi-porous radial microcrack network within each platelet extends to the steel interface. There are about 500 to 1500 microcracks extending to the substrate per platelet, or about 20 to 40 microcracks per cross-sectional platelet face extending to the interface. The microcrack network provides an even larger cross-sectional path for thermochemical degrading combustion gases to form approximately 500 to 1500 microvoids per platelet in their exposed steel interface at the base of the microcracks. These microvoids are filled with a semi-metallic to nonmetallic interfacial oxidization layer. Although there is nearly no convective heating in these very narrow cracks, the substrate steel at the base of these microcracks reacts with the high-pressure combustion gases for as long as the substrate steel temperature is above a given reaction threshold. These interfacial microvoids are extensive and reduce platelet-substrate adhesion across the entire cross-sectional area of the platelet-substrate interface. These oxidation layer-filled microvoids at the base of a platelet's microcrack network partially detach the chromium platelet from the steel substrate at about 500 to 1500 cross-sectional interfacial points, and it does not matter whether the microvoid thicknesses are each a thousand, million, or billon atoms thick since the adhesion is still zero at any atomic thickness. Interfacial microvoid link-up across the platelet cross-sectional area accelerates the loss of platelet-substrate adhesion leading to platelet spalling. These combustion gas paths include the entire cross-sectional area of the platelets. Each round fired provides a fresh volume of thermochemical degrading high-pressure gases to fill each radial microcrack extending to the steel interface within these platelets. Polished bore cross-sections of networks of radial microcracks within platelets and thermochemically damaged steel substrate microvoids at the base of these microcracks typically require 1000x magnification.

Similarly, but much more infrequently, LC chromium plate's semi-porous radial microcrack network within each platelet extends to the steel interface. There are about 10 to 15 microcracks extending to the substrate per platelet, or about 3 to 4 microcracks per cross-sectional platelet face extending to the interface. This microcrack network provides a somewhat larger cross-sectional path for thermochemical degrading combustion gases to form approximately 10 to 15 microvoids per platelet in their exposed steel interface at the base of these microcracks. Low contraction chromium plate adhesion is compromised by these interfacial steel microvoids.

These heat-checking cracks form interconnecting "canyons," and each round fired provides a high-velocity flow of the turbulent degrading combustion gases (gas wash flow) across the substrate steel at the base of the canyons that continuously refreshes the exposed interfacial surface. Combustion gas degradation forms voids in the exposed substrate steel that progressively enlarge with extended firing. Overhanging portions of chromium platelets above these voids crack and break off since the unsupported overhanging portion of a chromium platelet is brittle and the supported nonoverhanging portion of the chromium platelet is still attached to the substrate. There is slightly reduced projectile obturation near the origin in the "canyons" of these widened cracks, thus allowing combustion gases to briefly reach high velocities in these canyons as the projectile passes.

Progressive thermochemical degradation and gas washing (removal) of the exposed interfacial steel substrate surfaces in these "canyons" of the widened cracks result in the removal of unsupported HC chromium directly above these "canyons." The HC chromium is brittle, and its unsupported pieces above the widened "canyons" and the adjacent degraded steel walls of the "canyons" result in the breaking away of unsupported HC chromium pieces from any HC chromium pieces that still have partially nondegraded steel interfaces. Forces, such as high velocity flow and constrained thermal bore expansion of the HC chromium platelets, assist in the brittle failure-removal of unsupported HC chromium pieces above these "canyons" and their adjacent degraded walls. This results in further widening of the "canyons," an increase in interfacial convective heating, and an acceleration of the erosion process. This acceleration of the erosion process eventually leads to the complete degradation of the interfacial steel substrate under an HC chromium platelet. The spallation of an HC chromium platelet results in a micropit.

Yet another erosion mechanism component is micropitting onset that sets the stage for progressively wider and deeper pit growth. This pit growth is due to an exponential increase in interfacial convective heating and steel gas washing, and results in a rapid acceleration of the erosion process. For this zone six charge case, this thermochemical mechanism is the same for lands experiencing a 1 rph firing rate, lands experiencing an 8 rpm firing rate, grooves experiencing a 1 rph firing rate, grooves experiencing an 8 rpm firing rate, and only varies by heating rate from firing rate. For this zone six charge case with HC chromium coating and an 8 rpm firing rate, the rate of groove erosion far exceeds the rate of land erosion as shown in tubes 8, 9, and 12. Conversely, for this zone six charge case with HC chromium coating and a 1 rph firing rate, the rate of land erosion far exceeds the rate of groove erosion as shown in tubes 2, 7, and other tubes that experienced this slow firing rate. In addition, there is a mechanical mechanism component to driving edge land erosion that is qualitatively addressed in this effort.

With extended firing, HC chromium pits form due to platelet spalling providing a massive cross-sectional path for thermal and thermochemical degrading combustion gases to reach the exposed steel interface. High contraction chromium pits form due to platelet spalling. Each round fired provides a high velocity flow of these turbulent degrading combustion gases (gas wash flow) across the substrate steel at the base of these pits that continuously refreshes the exposed interfacial surface.

Another erosion mechanism component is the transformation of the steel substrate. At 1340°F, there is a transformation onset of the steel substrate. This steel substrate heat-affected zone also requires more volume then the untransformed steel and applies an upward force on HC chromium platelet that assists spalling.

Another erosion mechanism component is the oxidation of the exposed interfacial steel substrate. If the substrate at the base of a radial HC chromium crack or pit is above a particular oxidation threshold, then a gas/wall chemical reaction occurs until the exposed substrate wall temperature drops below the threshold. This forms a semi-metallic to nonmetallic ceramic-like oxidization layer on the exposed steel. The oxide layer cracks with thermal expansion, contraction, expansive flaking oxidation, and firing shock. During the next firing and filling of combustion gases, the gas passes through the cracked oxide layer to the exposed steel surface.

Exposed interfacial steel preferentially oxidizes due to the higher energy state of the interface bonds at the substrate base of heat-checking cracks, at the substrate base of the microcrack network within a platelet, and at the substrate base of pits.

At about 1340°F, there is an accelerated expansive flaking scale-type oxidation onset of iron by oxygen. Gases oxidize (oxidation, sulfidation) the exposed interface steel as long as the substrate wall temperature is above this required threshold. This oxide layer takes up more volume then when it is a metal forming a nonmetallic void in the steel at the interface. This void is filled with a poorly attached semi-metallic to nonmetallic interfacial oxidization layer between the steel and the chromium that pushes up on the HC chromium platelets. When voids at the substrate base of a heat-checking crack is filled with a semi-metallic to nonmetallic interfacial oxidization layer, then it reduces platelet-substrate adhesion around the interfacial edges of the platelet-substrate interface and applies an upward force on the platelet that assists spalling. When microvoids at the substrate base of a microcrack network within a platelet are filled with semi-metallic to nonmetallic interfacial oxidization layers, then it reduces platelet-substrate adhesion across the entire cross-sectional area of the platelet-substrate interface and applies an upward force on the platelet that assists spalling. Spalling of a chromium platelet produces a micropit that accelerates adjacent platelet spalling and eventually produces a larger pit.

Oxidizing combustion gas products travel down chromium plate microcracks, cracks, micropits, and pits to the exposed substrate steel. On top of the steel substrate's heat-affected zone is a carburized white layer. On top of this steel substrate's carburized white layer is a nonmetallic to semi-metallic layer of steel (iron) oxidation products. We have often measured the above oxygen and sulfur percentages in these oxidized layers and found that they are similar for advanced artillery, tank, and medium caliber gun systems. We also found that white layer and the steel substrate heat-affected zone are much lower in oxygen and sulfur content, since oxygen and sulfur diffuse poorly into these regions. Typical oxidized steel layers consist of approximately 10 to 50% oxygen as iron oxides and may also consist of approximately 1 to 10% sulfur as iron sulfides. As exposed substrate steel surfaces are degraded, iron atoms migrate to the surface from within, leaving a defect-laden metal matrix under the oxide layers. Erosion accelerates if the iron oxides or iron sulfides in these oxidation layers melt.

Another erosion mechanism component is carburization of the exposed interfacial steel substrate. Carburized combustion gas products travel down chromium plate microcracks, cracks, micropits, and pits to the exposed substrate steel. On top of the steel substrate heat-affected zone is a white layer consisting of an iron carbide white layer eutectic. This white layer is metallic steel substrate with thermal and diffusion damage. We have often measured the above carbon percentages in these white layers, steel substrate heat-affected zone, and virgin steel below the heat-affected zone, and found that they are similar for artillery, tank, and medium caliber gun systems. We also found that the phase change (martensite to untempered martensite) producing the steel substrate heat-affected zone enhances carbon diffusion into this region. The virgin steel substrate contains roughly a third of a percent of carbon. Typical steel white layers consist of approximately 10% carbon as iron carbide eutectic. Typical steel substrate heat-affected zone consists of less than 1% to almost 10% carbon. Exposed steel is highly degraded at surface, and a decreasing carbon diffusion gradient damages the steel below the surface. Erosion accelerates if the iron carbide eutectic in the white layer melts.

Another erosion mechanism component is obturator blowby and accelerated groove erosion during the first six inches of travel, producing reduced erosion life due to higher rate of fire scenarios. Never before seen rapid firing-induced groove erosion apparently caused this gun system's prototype XM297 cannon to erode to condemnation in less than a tenth of its expected life. The reduced erosion life at higher rate of firing scenarios is due to obturator blowby that causes accelerated groove erosion during the first six inches of travel.

Our finite element analysis studies of this gun system during top-zone rapid firing indicate that high-pressure-induced tube dilation is high, and this reduces the nominal obturator's ability to reach and seal to the bottom of the grooves during the first six inches of travel. Similar studies of this gun system during top-zone lower rate of firing indicate that high-pressure-induced tube dilation is lower, and this increases the nominal obturator's ability to reach and seal to the bottom of the grooves during the first six inches of travel. These studies indicate that it takes less than 1-inch to up to 6-inches of travel for the obturator to fully seal the bottom of the grooves due to obturator high-pressure deformation and thermal softening depending on the firing rate-induced tube dilation. These studies are based on interior ballistic core flow, properties of the nominal obturator, and measured dilation data.

Our nondestructive magnifying borescope studies and destructive metallographic studies indicate near-origin groove heating significantly exceeds the heating that results from the nonblowby, full obturation condition and can easily equal the heating that would result from the blowby less-than-full obturation condition. These studies are based on microcrack widths, heat-checking crack widths, substrate degradation, and chromium loss.

Numerous concepts are being tried to reduce zone six, rapid firing-related origin erosion. Improved obturators are being developed that should fully seal the bottom of the grooves in less than 1-inch during zone six, rapid firing thus minimizing near-origin groove erosion. Improved bore coating material is being developed that should resist near-origin groove erosion longer during zone six, rapid firing. Cooling the bore with a water-glycol mixture is four seconds late for reducing the maximum origin wall temperature that determines the erosion rate, but this bore cooling does allow more high rate of fire rounds to be fired before the charge cook-off temperature is reached. Current modular artillery charge ablatives are not very effective at reducing the maximum origin wall temperature that determines the erosion rate. Rear-notched ablative obturators are being developed that should reduce the maximum origin wall temperature that determines the erosion rate by deploying ablative at the origin where it is needed and not from the chamber. We have previously determined ablative mechanisms, erosion models, and erosion predictions for a number of advanced artillery, tank, and medium caliber gun systems.

Figures 10 and 11 show micrographic examples of nondestructive substrate exposure measurements taken by a 70x magnifying borescope with a calibrated scale. Using this technique, these and similar micrographs illustrate the progression of this gun system's erosion at a low and high rate of fire. Figure 10 shows typical midlife driving edge land erosion for this zone six charge at 47 inches from the RFT, 10:00 to 2:00 clock positions, and 1 rph firing rate. In this figure, coppering is evident, HC chromium loss is about 50%, and gas washing has produced moderately deep measured pits. Figure 11 shows typical midlife groove erosion for this zone six charge at 47 inches from the RFT, 10:00 to 2:00 clock positions, and 8 rpm firing

rate. In this latter figure, mean HC chromium loss is about 50% in this area, but less than that in this micrograph, and gas washing has produced moderately deep measured pits. As we have seen in previous work, the high velocity reacting gases progressively wash and widen the interconnected canyons and form extending voids in the dead-end areas. As we have also seen in previous work, at the midlife stage, the unsupported HC chromium plate breaks off where it is unsupported. Comparatively, HC chromium platelets are smaller on the land driving edge at the minimum 1 rph firing rate than they are in the grooves at the maximum 8 rpm firing rate.

Figure 12 shows a micrograph from this gun system with typical 47-inch from RFT, 10:00 to 2:00 clock positions, and land and groove steel substrate erosion through a microcrack. This destructive substrate exposure characterization is from an SEM, although similar characterizations were made by a metallograph. This and other cross-sections were taken away from groove pits and land pits at middle tube life, 47-inch from RFT position, and at 2000x. The inverted triangles (about 15- x 15-μm) in the steel substrate are almost universally present at the base of the fine HC chromium crack (about 1-μm wide) for both land and groove erosion, although their rate of erosion varied with the zone six charge firing rate. The damage to this steel substrate is caused by high-pressure combustion gas filling from each round. To put into perspective the small size of the inverted triangles and crack width, the HC chromium plate thickness is about 130-μm. In addition, typical land and groove interface degradation and voids are present in this figure to the right of the inverted triangle. This figure shows the initiation of erosion that progresses and accelerates with HC chromium crack widening, substrate steel interfacial damage, HC chromium platelet spalling, micropitting enlargement to macropitting, and substrate steel gas washing to condemnation.

Using coupled chemical analysis techniques, characterizations of the micrographic region shown in Figure 12, and other similar micrographic regions, show phase change degradation (diffusion-induced carburized white layer and heat-affected zone on/into exposed gun steel, chromium recrystallization) and chemical reaction degradation (oxygen and sulfur oxidation of exposed gun steel forming semi-metallic layers) of the gun steel substrate under the HC chromium plate at crack and interfacial walls/wall layers.

For this gun system, Figures 13 through 15 show respective maximum wall temperature (T_{wall}) predictions for the reacting HC chromium surface, unexposed-reacting steel substrate interface through an HC chromium crack, and exposed-reacting steel substrate surface due to HC chromium spalling in pits wider than they are deep. In these three figures, maximum T_{wall} data for this gun system are shown versus selected axial positions for the first, eighth, and fifteenth rounds of an 8 rpm firing rate. The 1 rph firing rate would be the same as the first round of an 8 rpm firing rate if only one round were fired per hour. In these figures, maximum values were shown instead of calculated time-dependent data to compare the rounds in the 15-round groups.

For Figure 13, the maximum wall temperatures shown for the HC chromium surface did not result in HC chromium reactions or phase changes, thus explaining their inertness. As a result, the reacting HC chromium surface temperatures in Figure 13 are very similar to the nonreacting HC chromium surface temperatures in Figure 4.

For Figures 14 and 15, this gun system's MACE maximum wall temperatures shown for both the unexposed reacting gun steel interface and the fully exposed reacting gun steel surface did result in steel substrate reactions and phase changes, thus explaining their reactivity. For the first round fired in Figure 14, the steel transformation and oxidation onset temperature ($T_{t\text{-}ox}$) of about 1340°F is exceeded from the origin to about six inches of travel. For the eighth and fifteenth rounds fired in Figure 14, the steel $T_{t\text{-}ox}$ of about 1340°F is exceeded from the origin to about two feet of travel. For the first round fired in Figure 15, the steel $T_{t\text{-}ox}$ of about 1340°F is exceeded from the origin to about four feet of travel. For the eighth and fifteenth rounds fired in Figure 14, the steel $T_{t\text{-}ox}$ of about 1340°F is exceeded from the origin to about six feet of travel.

Our nonreacting thermal predictions using FDHEAT deviate from our reacting thermal/thermochemical predictions using MACE only at axial positions where bore erosion occurred. In this gun system, erosion occurred in the first six inches of travel and gas/wall reactions involving the steel substrate above 1340°F wall temperature thresholds raised the wall to higher temperatures than pure thermal calculations would predict.

Data from Figures 8 and 9 and 13 through 15 are used to calibrate and predict resultant substrate interface temperatures for the various exhibited crack/pit widths using a cubic function discussed previously (ref 6). These data include the fully convective/exposed surface heating cases from Figures 13 and 15, and the fully conductive/unexposed substrate interface heating case from Figure 14, and substrate exposure data from Figures 8 and 9. Using this cubic function, Figure 16 shows the substrate interface temperatures for the various exhibited crack/pit widths for this gun system at the 47-inch from RFT position. The data consist of the maximum exposed interface temperature as a function of HC chromium plate crack/pit width at the first, eighth, and fifteenth rounds of an 8 rpm firing rate. As a given crack or pit widens, the increased convective heating exponentially raises the maximum wall temperature of the exposed substrate steel interface at the pit base and also exponentially raises its associated erosion rate. For all these various exhibited crack and pit widths at this peak eroded position, the first, eighth, and fifteenth rounds of an 8 rpm firing rate all exceeded the steel $T_{t\text{-}ox}$ of about 1340°F.

These resultant substrate interface temperatures for given crack/pit widths correlate and have been successfully applied to numerous advanced medium and large caliber gun systems, based on measured firing-related data from their most extreme rounds. The measurements include phase change degradation data (diffusion-induced carburized white layer and heat-affected zone on/into exposed gun steel, chromium recrystallization) and chemical reaction degradation data (oxygen and sulfur oxidation of exposed gun steel forming semi-metallic layers). The existence and depth of the measured degradations into exposed gun steel substrate depends on and correlate with the magnitude of the related positional-dependent wall temperature profiles. The measurements were focused on the exposed gun steel substrate at the crack/pit/interface walls and wall layers.

Surface ablation rates are calculated directly by the MACE model. The MACE model also uses the resultant substrate interface temperatures in cracks/pits to calculate the substrate interface ablation rates as a function of position, time, and rounds. This is done for the life of each crack and pit. The exposed steel interface degradation (transformation, interstitial occupation, reactions) under a chromium platelet is consumed by the associated ablation rate

above the ablation threshold. When void and microvoid degradation of the exposed gun steel interface thickness under this coating platelet merges with all adjacent degradation, then the coating platelet spalls and gas wash onset begins.

The HC chromium plate has a passivating oxidation at about 3140°F and a melting point at about 3370°F, both of which explain its inertness. Steel substrate degradation of interfaces, cracks, pits, and surfaces is computed by the area under a temperature-time curve above a degradation threshold such as:

- The 1340°F transformation onset of steel
- The 1340°F accelerated expansive flaking scale-type oxidation onset of iron by oxygen
- The 1340°F accelerated diffusion onset of carbon into steel to Fe3C
- The 1830°F accelerated oxidation onset of iron by sulfur
- The 2100°F melting point onset of iron carbide white layer eutectic
- The 2190°F melting point onset of this iron-sulfur compound
- The 2490°F melting point onset of the iron-oxygen compound
- The 2640°F melting point onset of gun steel

For this HC chromium Crusader gun system modeling effort, peak unexposed steel substrate temperatures are about 1460°F. For this same effort, peak exposed (cracks, pits) steel substrate temperatures are about 1640°F. The only types of substrate steel degradation that apply to this gun system include the 1340°F transformation onset of steel, 1340°F accelerated expansive flaking scale-type oxidation onset of iron by oxygen, and 1340°F accelerated diffusion onset of carbon into steel to Fe3C. Hydrogen interstitials also play an undetermined role in this HC chromium and substrate steel degradation.

Figure 17 shows this gun system's maximum wall temperature at the 47-inch from RFT axial position for a 15-round group at 8 rpm. The five curves include the bore surface temperature at firing (T_{bf}), the 400°F cook-off temperature (T_{co}), the steel substrate transformation and oxidation onset temperature ($T_{t\text{-}ox}$), the unexposed interfacial steel substrate temperature (T_i), and the HC chromium bore surface temperature (T_b). The cook-off temperature is not reached for the 15-round group at 8 rpm. Similarly, all unexposed interfacial steel substrate maximum temperatures exceed the 1340°F steel substrate transformation, accelerated oxidation, and accelerated carbon diffusion onset temperatures.

For erosion at the 12:00 wall (10:00 to 2:00), Figure 18 gives this gun system's MACE cumulative erosion predictions at the peak eroded 47-inch origin position for the respective recurring 1 rph single-round firing scenario, 2 rpm recurring rapid-firing scenario, 4 rpm recurring rapid-firing scenario, 6 rpm recurring rapid-firing scenario, and 8 rpm recurring rapid-firing scenario. Rapid firing scenarios consist of recurring groups of 15 rounds. For erosion at the 12:00 to 6:00 diameter and to add further balance to the results, Figure 19 gives similar type cumulative erosion predictions as in Figure 18 for the same five recurring firing scenarios at the peak eroded 47-inch origin position. The recurring 1 rph single-round firing scenario is dominated by peak origin land erosion, while the recurring 8 rpm for 15-round groups firing

scenario is dominated by peak origin groove erosion, and the intermediate firing rates are dominated by a mixture of peak origin land and groove erosion.

For the peak origin erosion at the 12:00 wall (10:00 to 2:00) in Figure 18, we predict that it requires approximately 1520, 1510, 1390, 1070, and 450 respective EFCs to achieve arbitrary 0.100-inch origin wall erosion 1 rph, and 2, 4, 6, and 8 rpm firing scenarios. For the peak origin erosion at the 12:00 to 6:00 diameter in Figure 19, we predict that it requires approximately 1005, 995, 930, 750, and 400 respective EFCs to achieve an arbitrary 0.100-inch origin diameter erosion for these same five respective firing scenarios. For the peak erosion at the 12:00 origin wall (10:00 to 2:00) and at the 12:00 to 6:00 origin diameter in these figures, we further predict that it requires approximately 330, 325, 300, 240, and 120 respective EFCs to achieve steel substrate gas wash onset for these five respective firing scenarios.

Typical 155-mm HC chromium plated artillery cannons have an erosion delay before exponential origin erosion occurs that may or may not slow toward a limiting value due to pitting-type erosion. Conversely, typical 155-mm bare steel artillery cannons immediately start with exponential origin erosion that usually slows toward a limiting value due to nonpitting-type progressive erosion.

Key peak eroded HC chromium Crusader tubes referenced in this report were near the end of their erosion life, nondestructively inspected periodically throughout their lives, and finally destructively characterized, resulting in moderately high-confidence erosion predictions. Key peak eroded HC chromium Crusader tubes, such as tubes 2, 7, and others, fired up to 945 equivalent EFCs based on the recurring 1 rph single-round rate and had up to 0.095-inch origin land diameter erosion at 12:00 to 6:00, 0.070-inch origin land erosion at 12:00 wall (10:00 to 2:00), 0.025-inch origin land erosion at 6:00 wall (4:00 to 8:00), and had a fraction of each of these three numbers on their origin grooves. Key peak eroded HC chromium Crusader tubes such as tubes 8, 9, and 12, fired up to 355 equivalent EFCs based on the recurring 8 rpm for 15-round group rate (390 total EFCs), and had up to 0.088-inch origin groove diameter erosion at 12:00 to 6:00, 0.080-inch origin groove erosion at 12:00 wall (10:00 to 2:00), 0.008inch origin groove erosion at 6:00 wall (4:00 to 8:00), and had a fraction of each of these three numbers on their origin lands.

Left of the black lines in Figures 18 and 19 represents the portion of the HC chromium Crusader predictions that result from the calibrated erosion model, based on the reduction of actual firing, inspection (star gage, magnifying borescope), and characterization data. Right of the black lines in Figures 18 and 19 represents the portion of the HC chromium Crusader predictions that result from the extension of the calibrated erosion model, based on the same actual firing, inspection, and characterization data.

Crusader tubes referenced in this report had 0.0050-inch HC chromium plated on both the lands and grooves. For the peak origin erosion at the 12:00 wall (10:00 to 2:00) in Figure 18, we predict that it requires approximately 1520 and 450 respective EFCs to achieve arbitrary 0.100-inch origin wall erosion for the recurring 1 rph single-round, and the recurring 8 rpm for 15-round firing scenarios. For the peak origin erosion at the 12:00 to 6:00 diameter in Figure 19, we

predict that it requires approximately 1005 and 400 respective EFCs to achieve arbitrary 0.100-inch origin diameter erosion for these same two respective firing scenarios.

The actual number of EFCs it took the key peak eroded HC chromium plated Crusader tubes fired at the lowest firing rate to get to a 20% erosion life depth (either 12:00 wall or 12:00 to 6:00 diameter) is approximately equal to the actual number of EFCs it took the key peak eroded HC chromium plated Crusader tubes fired at the highest firing rate to get to a near-end of life erosion depth (either 12:00 wall or 12:00 to 6:00 diameter).

Also, the predicted number of EFCs it took the key peak eroded HC chromium plated Crusader tubes fired at the lowest firing rate to get to an arbitrary 0.100-inch erosion depth (either 12:00 wall or 12:00 to 6:00 diameter) is more than twice the predicted number of EFCs it took the key peak eroded HC chromium plated Crusader tubes fired at the highest firing rate to get to an arbitrary 0.100-inch erosion depth (either 12:00 wall or 12:00 to 6:00 diameter).

By both actual firing and computational modeling, it appears that key peak eroded HC chromium Crusader tubes fired at the lowest firing rate outperformed by more than a factor of two the key peak eroded HC chromium Crusader tubes fired at the highest firing rate.

Figure 20 shows a typical tube #2 magnifying borescope photo with near-end of life erosion at 47 inches from RFT, 10x, 12:00, zone six max, and 1 rph max firing rate, with significant land erosion and minimal groove erosion. Figure 21 shows a typical tube #8 magnifying borescope photo with near-end of life erosion in at 47 inches from RFT, 10x, 12:00, zone six max, and 8 rpm max firing rate, with significant groove erosion and minimal land erosion.

Figure 22 shows a typical tube #2 magnifying borescope photo with near-end of life erosion in at 47 to 53 inches from RFT, 360 degree view, zone six max, and 1 rph max firing rate, with significant 10:00 to 2:00 o'clock land erosion and minimal 10:00 to 2:00 o'clock groove erosion. Figure 23 shows a typical tube #8 magnifying borescope photo with near-end of life erosion in at 47 to 53 inches from RFT, 360 degree view, zone six max, and 8 rpm max firing rate, with significant 10:00 to 2:00 o'clock groove erosion and minimal 10:00 to 2:00 o'clock land erosion.

In summary, thermal-chemical-mechanical erosion modeling predictions are given for the HC chromium plated Crusader gun system based on extensive cannon firing, inspection, characterization, and experimental data. This effort was conducted for the Army's Crusader Program Manager Office. Most key cannons were near their provisional diametric erosion limit, and were destructively characterized resulting in moderately high-confidence erosion mechanism determinations and erosion predictions.

REFERENCES

1. Dunn, S., Sopok, S., Coats, D., O'Hara, P., Nickerson, G., and Pflegl, G., "Unified Computer Model for Predicting Thermochemical Erosion in Gun Barrels," *Proceedings of 31st AIAA Joint Propulsion Conference*, San Diego, CA, July 1995; Also *AIAA Journal of Propulsion and Power*, Volume 15, Number 4, pp. 601-612.

2. Coats, D., Dunn, S., and Sopok, S., "A New Chemical Equilibrium Code with Compressibility Effects," *Proceedings of the 33rd JANNAF Combustion Meeting*, Monterey, CA, October 1996, pp. 1-10.

3. Gough, P., "The XNOVAKTC Code," Paul Gough Associates, Portsmouth, NH, U.S. Army BRL-CR-627, February 1990. Developed and distributed by the Army Research Laboratory, APG, MD.

4. Levine, J., "Transpiration and Film Cooling Boundary Layer Computer Program (MABL) - Numerical Solution of the Turbulent Boundary Layer Equations with Equilibrium Chemistry," NASA Marshall N72-19312, June 1971; Also Dunn, S., "MABL Gun Model," Software and Engineering Associates, Inc., Carson City, NV, February 1992.

5. Dunn, S., "Materials Ablation Conduction Erosion Program (MACE)," Software and Engineering Associates, Inc., Carson City, NV, June 1989; Also Dunn, S., "Updated MACE Gun Model," Software and Engineering Associates, Inc., Carson City, NV, February 1992.

6. Sopok, S., "Cannon Coating Erosion Model with Updated M829E3 Example," *Proceedings of the 36th AIAA Joint Propulsion Conference*, Huntsville, AL, July 2000.

7. Rutkowski, J., private communication on the propelling charge, U.S. Army ARDEC, Dover, NJ, May-July 2002.

8. Underwood, J., Parker, A., Vigilante, G., Cote, P., "Thermal Damage, Cracking, and Rapid Erosion of Cannon Bore Coatings," *Proceedings of the Gun Tubes Conference 2002*, Keble College Oxford, UK, September 2002.

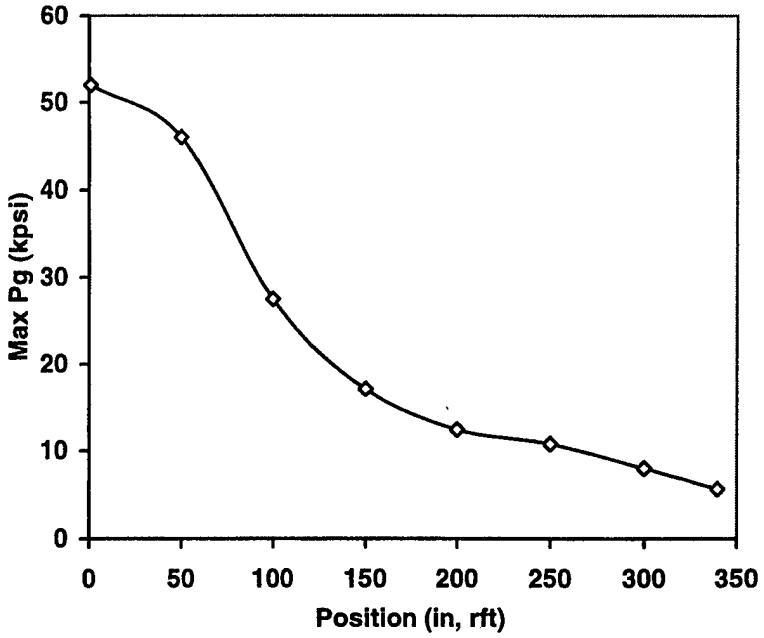

Figure 1. NOVA gas pressure.

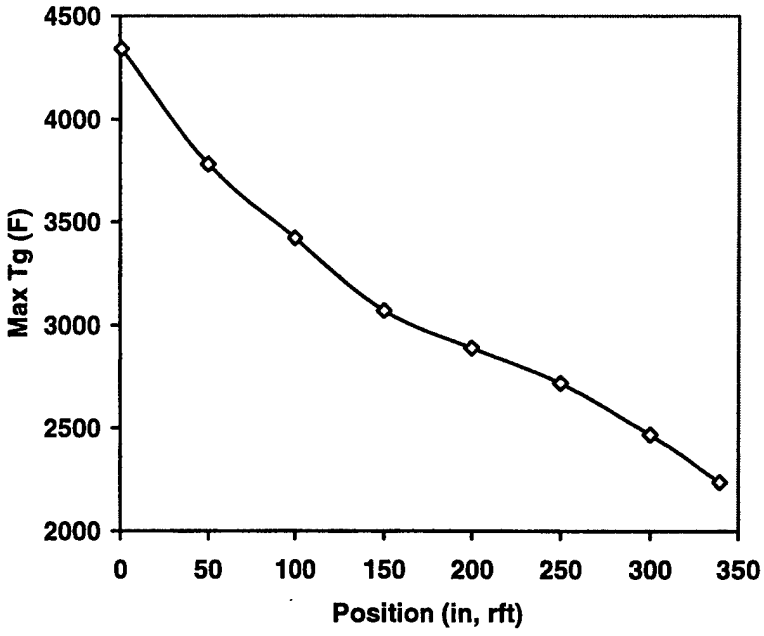

Figure 2. NOVA gas temperature.

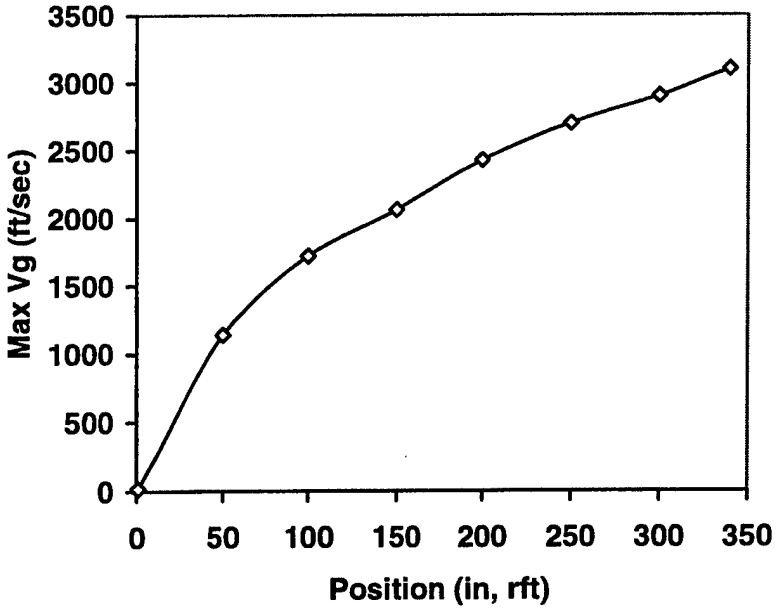

Figure 3. NOVA gas velocity.

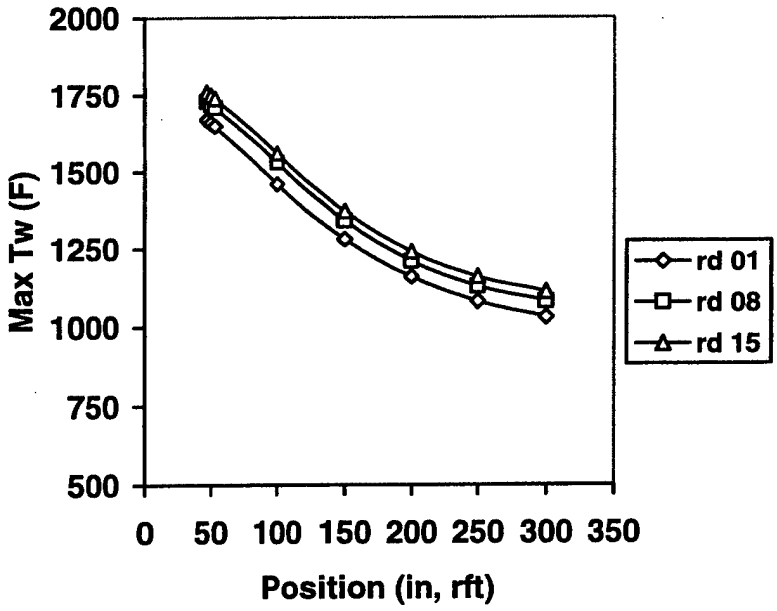

Figure 4. MACE nonreacting HC chromium thermal analysis at 8 rpm for rounds 1, 8, and 15.

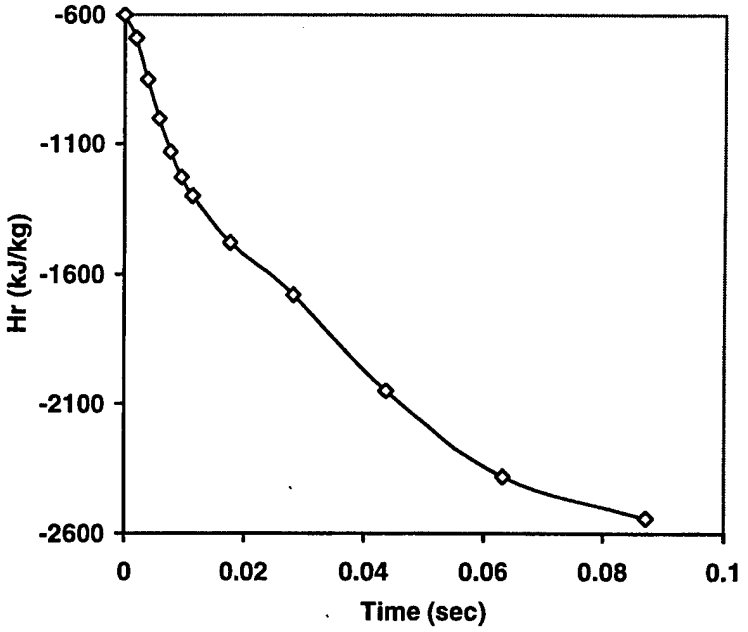

Figure 5. MABL recovery enthalpy at 47 inches from RFT.

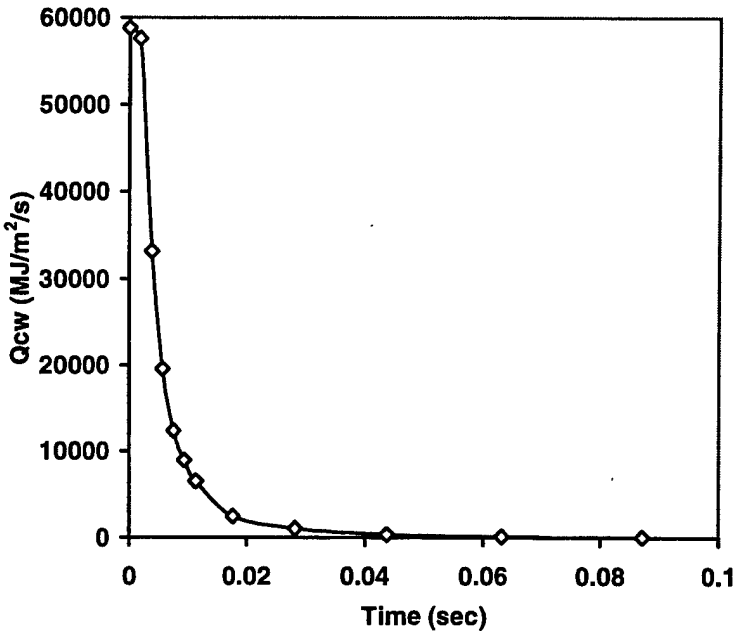

Figure 6. MABL cold wall heat flux at 47 inches from RFT.

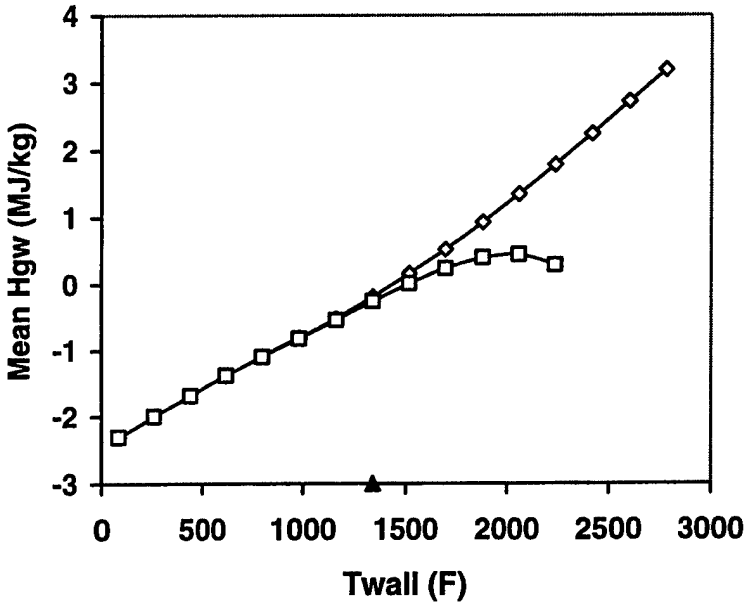

Figure 7. Gas/wall thermochemistry with $T_{t\text{-}ox}$
(legend: diamonds = HC chromium and squares = steel).

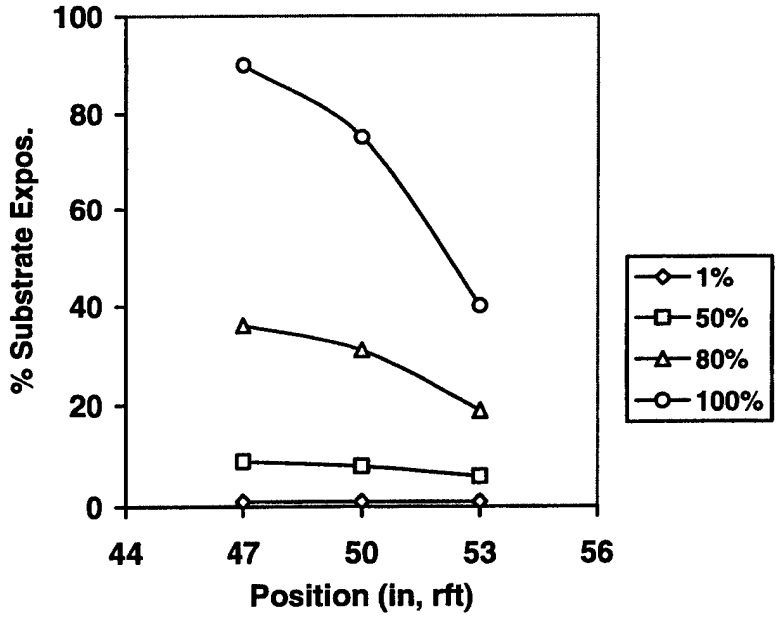

Figure 8. Groove substrate exposure versus selected axial position for 8 rpm and 10:00 to 2:00 position at 1, 50, 80, and 100% equivalent life.

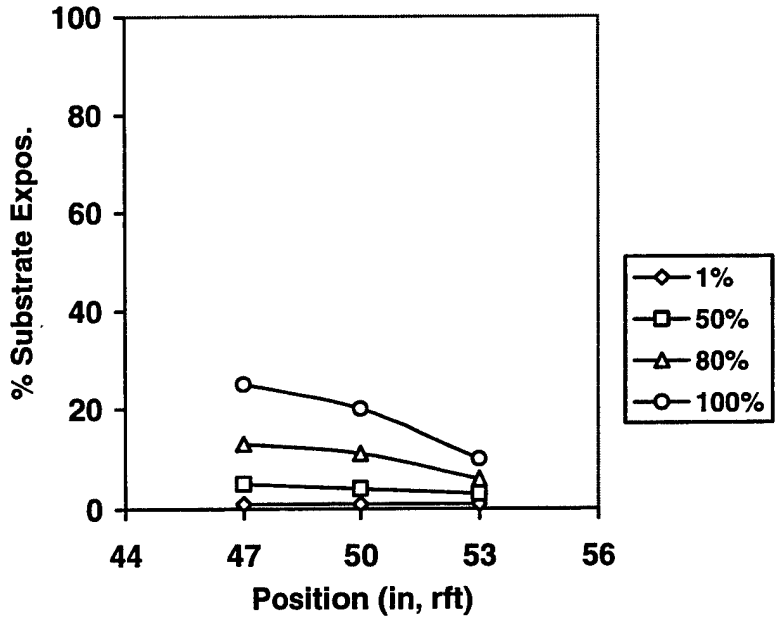

Figure 9. Land substrate exposure versus selected axial position for 1 rph and 10:00 to 2:00 position at 1, 50, 80, and 100% equivalent life.

Figure 10. Typical midlife land erosion by magnifying borescope at 47 inches from RFT, 10:00 to 2:00 , and 1 rph firing rate.

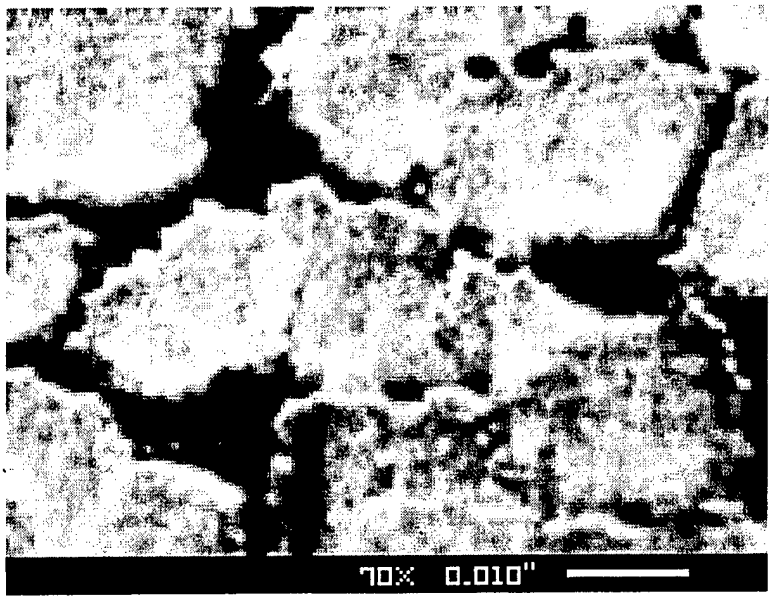

Figure 11. Typical midlife groove erosion by magnifying borescope at 47 inches from RFT, 10:00 to 2:00, and 8 rpm firing rate.

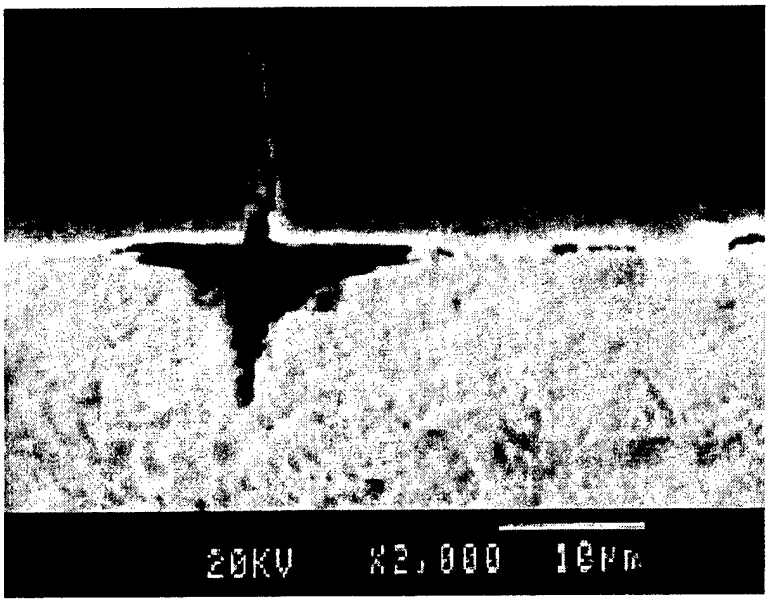

Figure 12. SEM cross-section of typical land and groove steel substrate erosion through a microcrack at 47 inches from RFT and 10:00 to 2:00 position.

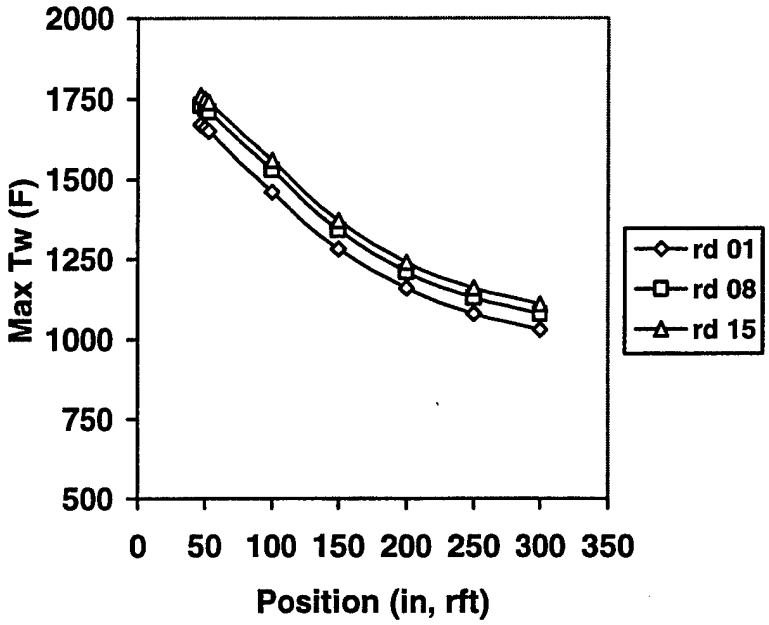

Figure 13. MACE reacting HC chromium surface temperatures for rounds 1, 8, and 15 at 8 rpm.

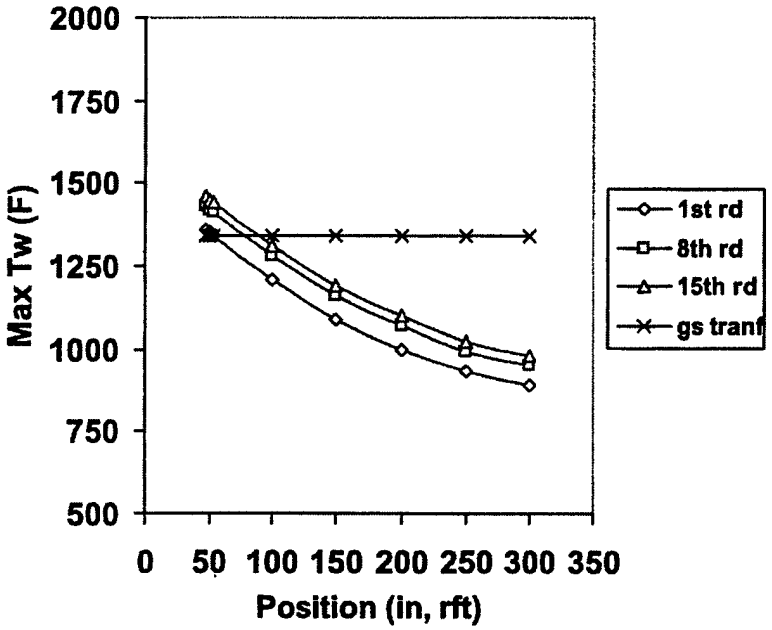

Figure 14. MACE unexposed reacting gun steel interface temperatures for rounds 1, 8, and 15, and steel $T_{t\text{-}ox}$ at 8 rpm.

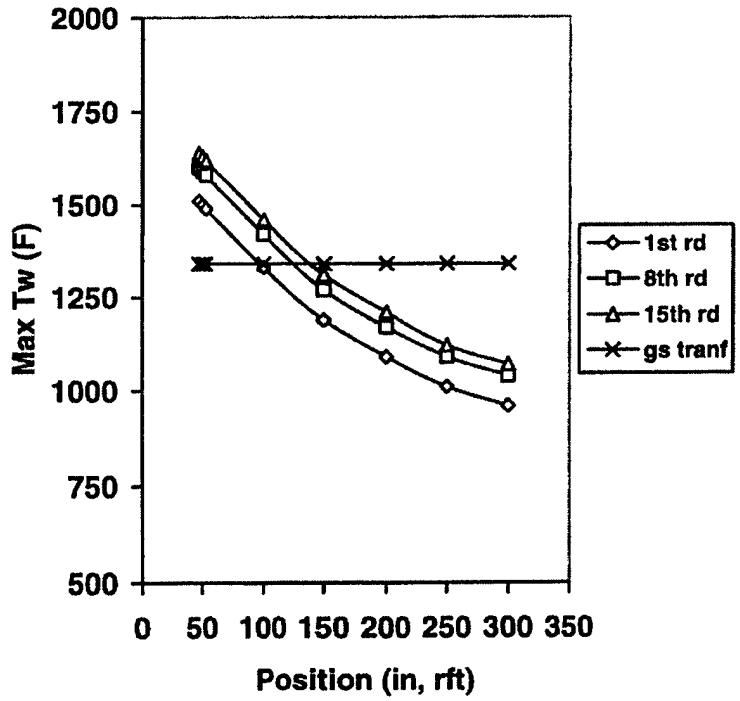

Figure 15. MACE fully exposed reacting gun steel surface temperatures for rounds 1, 8, and 15, and steel $T_{t\text{-}ox}$ at 8 rpm.

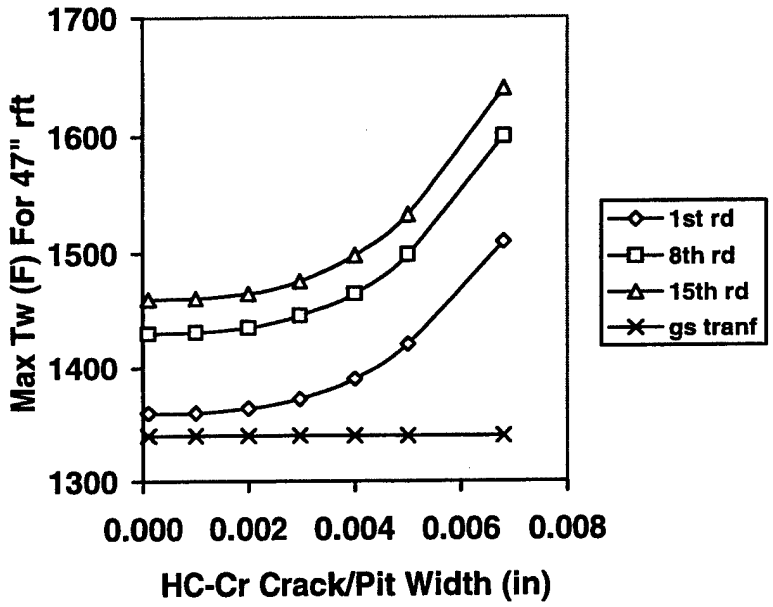

Figure 16. MACE exposed gun steel interface temperatures for rounds 1, 8, and 15, and steel $T_{t\text{-}ox}$ at 8 rpm.

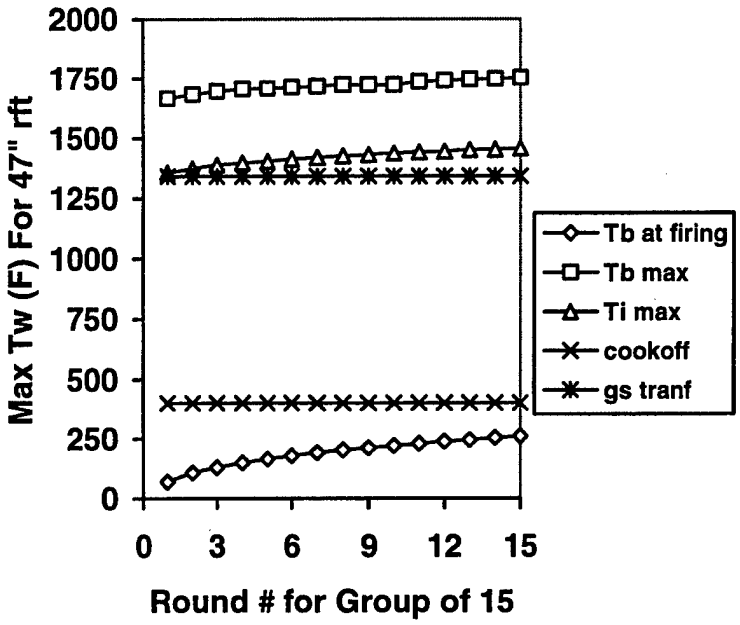

Figure 17. MACE reacting wall temperatures at the 47-inch from RFT axial position for a 15-round group at 8 rpm.

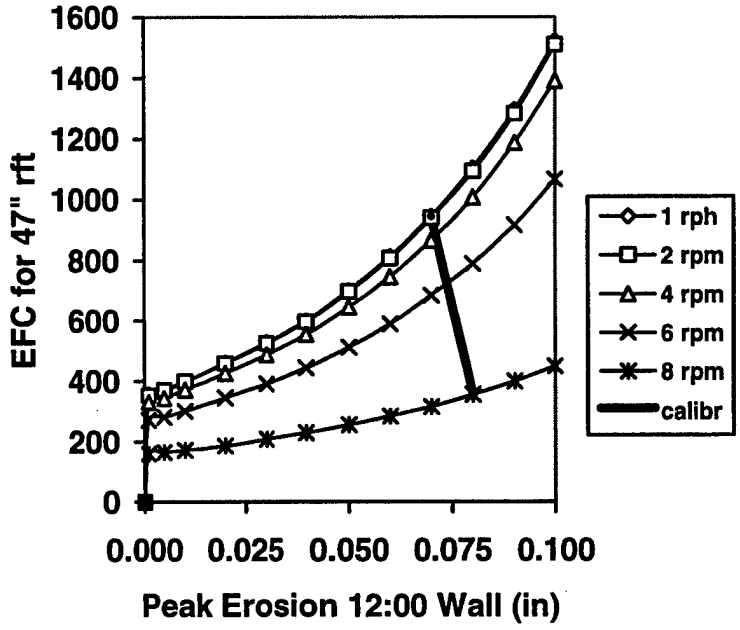

Figure 18. MACE cumulative 12:00 wall erosion predictions for 1 rph and 2, 4, 6, and 8 rpm firing scenarios.

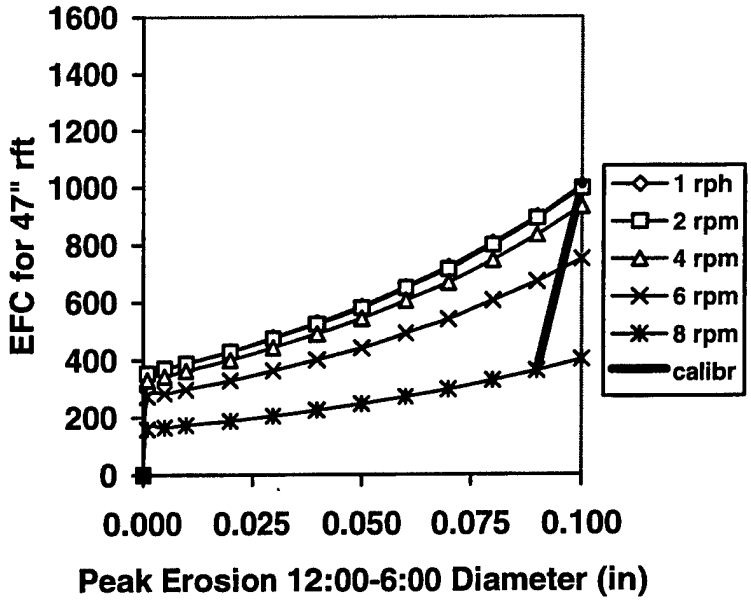

Figure 19. MACE cumulative 12:00 to 6:00 diameter erosion predictions for 1 rph and 2, 4, 6, and 8 rpm firing scenarios.

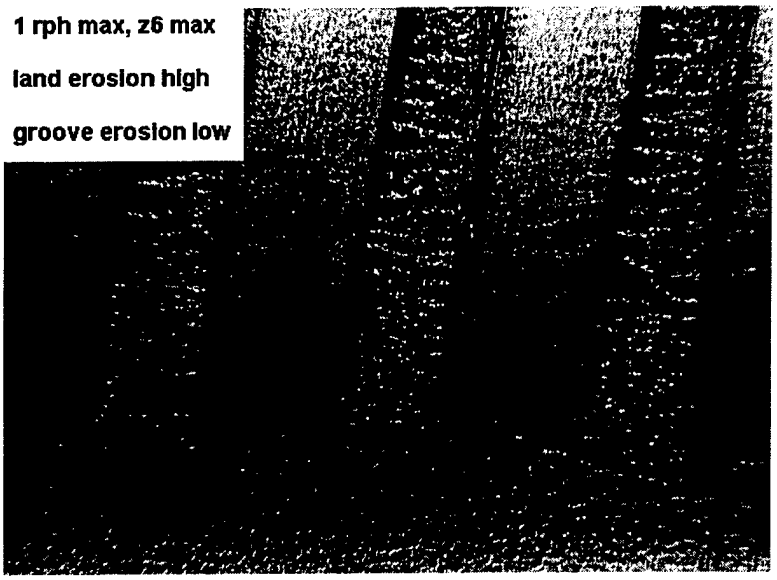

Figure 20. Typical near-end of life erosion by magnifying borescope at 47 inches from RFT, 10x, 12:00, zone six max, and 1 rph max firing rate.

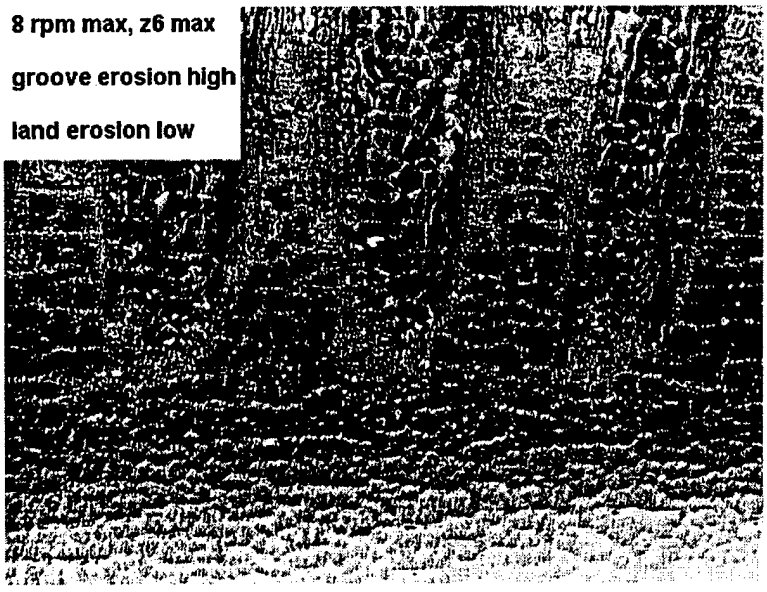

Figure 21. Typical near-end of life erosion by magnifying borescope at 47 inches from RFT, 10x, 12:00, zone six max, and 8 rpm max firing rate.

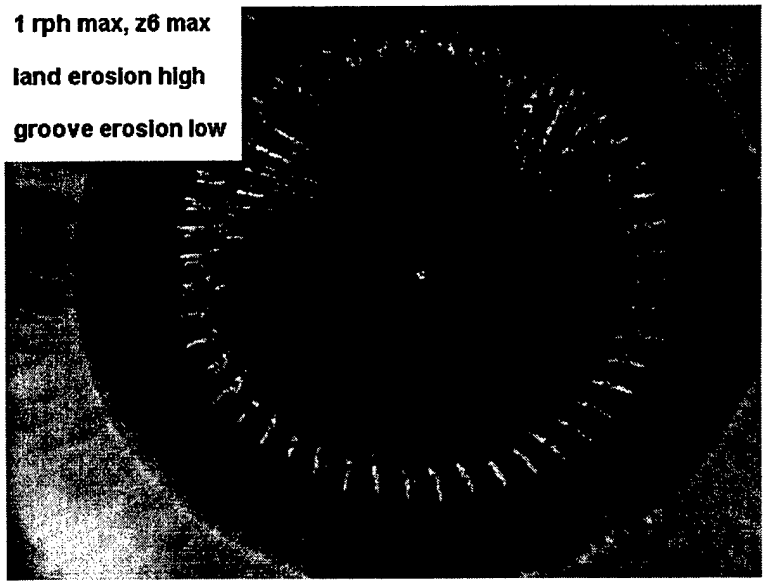

Figure 22. Typical near-end of life erosion by magnifying borescope at 47 to 53 inches from RFT, 360 degree view, zone six max, and 1 rph max firing rate.

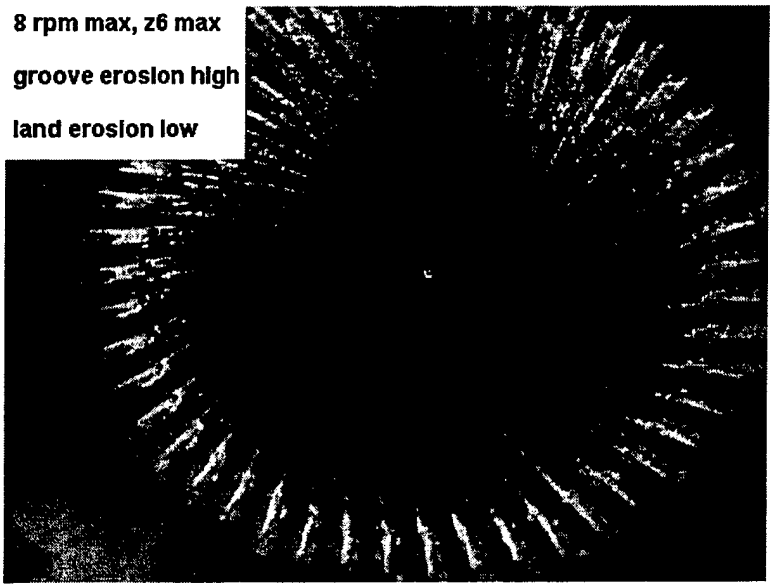

Figure 23. Typical near-end of life erosion by magnifying borescope at 47 to 53 inches from RFT, 360 degree view, zone six max, and 8 rpm max firing rate.

TECHNICAL REPORT INTERNAL DISTRIBUTION LIST

	NO. OF COPIES
TECHNICAL LIBRARY ATTN: AMSTA-AR-CCB-O	1
TECHNICAL PUBLICATIONS & EDITING SECTION ATTN: AMSTA-AR-CCB-O	3
PRODUCTION PLANNING & CONTROL DIVISION ATTN: AMSTA-WV-ODP-Q, BLDG. 35	1

NOTE: PLEASE NOTIFY DIRECTOR, BENÉT LABORATORIES, ATTN: AMSTA-AR-CCB-O OF ADDRESS CHANGES.

TECHNICAL REPORT EXTERNAL DISTRIBUTION LIST

	NO. OF COPIES
DEFENSE TECHNICAL INFO CENTER ATTN: DTIC-OCA (ACQUISITIONS) 8725 JOHN J. KINGMAN ROAD STE 0944 FT. BELVOIR, VA 22060-6218	2
COMMANDER U.S. ARMY TACOM-ARDEC ATTN: AMSTA-AR-WEE, BLDG. 3022 AMSTA-AR-AET-O, BLDG. 183 AMSTA-AR-FSA, BLDG. 61 AMSTA-AR-FSX AMSTA-AR-FSA-M, BLDG. 61 SO AMSTA-AR-WEL-TL, BLDG. 59 PICATINNY ARSENAL, NJ 07806-5000	 1 1 1 1 1 2
DIRECTOR U.S. ARMY RESEARCH LABORATORY ATTN: AMSRL-DD-T, BLDG. 305 ABERDEEN PROVING GROUND, MD 21005-5066	 1
DIRECTOR U.S. ARMY RESEARCH LABORATORY ATTN: AMSRL-WM-MB (DR. B. BURNS) ABERDEEN PROVING GROUND, MD 21005-5066	 1
CHIEF COMPOSITES & LIGHTWEIGHT STRUCTURES WEAPONS & MATLS RESEARCH DIRECT U.S. ARMY RESEARCH LABORATORY ATTN: AMSRL-WM-MB (DR. BRUCE FINK) ABERDEEN PROVING GROUND, MD 21005-5066	 1

	NO. OF COPIES
COMMANDER U.S. ARMY RESEARCH OFFICE ATTN: TECHNICAL LIBRARIAN P.O. BOX 12211 4300 S. MIAMI BOULEVARD RESEARCH TRIANGLE PARK, NC 27709-2211	 1
COMMANDER ROCK ISLAND ARSENAL ATTN: SIORI-SEM-L ROCK ISLAND, IL 61299-5001	 1
COMMANDER U.S. ARMY TANK-AUTMV R&D COMMAND ATTN: AMSTA-DDL (TECH LIBRARY) WARREN, MI 48397-5000	 1
COMMANDER U.S. MILITARY ACADEMY ATTN: DEPT OF CIVIL & MECH ENGR WEST POINT, NY 10966-1792	 1
U.S. ARMY AVIATION AND MISSILE COM REDSTONE SCIENTIFIC INFO CENTER ATTN: AMSAM-RD-OB-R (DOCUMENTS) REDSTONE ARSENAL, AL 35898-5000	 2
NATIONAL GROUND INTELLIGENCE CTR ATTN: DRXST-SD 2055 BOULDERS ROAD CHARLOTTESVILLE, VA 22911-8318	 1

NOTE: PLEASE NOTIFY COMMANDER, ARMAMENT RESEARCH, DEVELOPMENT, AND ENGINEERING CENTER, BENÉT LABORATORIES, CCAC, U.S. ARMY TANK-AUTOMOTIVE AND ARMAMENTS COMMAND, AMSTA-AR-CCB-O, WATERVLIET, NY 12189-4050 OF ADDRESS CHANGES.